

# A 28-year-long (1997–2024) hydrographic dataset from the southern Baltic Sea

Daniel Rak<sup>1</sup>, Anna Izabela Bulczak<sup>1</sup>, Waldemar Walczowski<sup>1</sup>, Piotr Wieczorek<sup>1</sup>, Małgorzata Merchel<sup>1</sup>, Robert Osiniński<sup>1</sup>, Ilona Goszczko<sup>1</sup>, Agnieszka Beszczynska-Moeller<sup>1</sup>, Agnieszka Strzelewicz<sup>1</sup>, Małgorzata Kitowska<sup>1</sup>

<sup>1</sup> Observational Oceanography Laboratory, Institute of Oceanology PAN, Physical Oceanography Department, Sopot, Poland

\* Correspondence to: Daniel Rak (rak@iopan.pl)

**Abstract.** The data set presented here consists of Conductivity–Temperature–Depth (CTD) observations collected during 96 research cruises of R/V *Oceania* across the southern Baltic Sea between 1997 and 2024. The collection comprises towed and vertical station profiles acquired along a repeat transect spanning the Arkona Basin, Bornholm Basin, Słupsk Furrow, and Gdańsk Basin. Acquisition and post-processing procedures include standardized parsing of CNV/TXT files, robust time/position handling, pressure-binning to 1 dbar, median filtering, automated geolocation quality control, and pruning of incomplete profiles. The dataset enables analyses of seasonal to decadal variability in temperature and salinity, inflow propagation, ventilation events, and model validation. Manufacturer specifications for the principal instruments (Guildline 87104, Idronaut OS316/OS316Plus, Sea-Bird SBE49, Sea-Bird SBE19plus) are summarized to inform uncertainty assessment.

## 1. Introduction

The Southern Baltic Sea, a semi-enclosed marginal sea, forms an important transitional region connecting the North Sea through the Danish Straits. This geographic setting leads to distinct hydrographic conditions characterized by episodic inflows of saline North Sea waters, which strongly influence stratification, deep-water renewal, and regional marine dynamics (Matthäus & Franck, 1992; Mohrholz et al., 2015). The proximity of the Danish Straits exerts a dominant control on hydrography in the region, as episodic inflows of saline North Sea water propagate eastward, shaping stratification and deep-water renewal. Consequently, this region exhibits pronounced vertical stratification patterns driven by inflow events and the progressive downstream modification of water masses with increasing distance from the Danish Straits, coupled with distinct seasonal variability in temperature and salinity (Leppäranta & Myrberg, 2009).

Major Baltic Inflows (MBIs), occur episodically from the North Sea into the Baltic Sea, significantly affecting its hydrography and circulation (Fischer & Matthäus, 1996; Mohrholz et al., 2015). These inflows are classified into two main types: barotropic and baroclinic. Barotropic inflows result primarily from large-scale meteorological forcing, such as prolonged westerly winds, significant changes in atmospheric pressure, and sea level differences between the North Sea and Baltic Sea, causing substantial volumes of saline water to enter the Baltic basins

35 (Burchard et al., 2005; Stigebrandt and Gustafsson, 2003). Baroclinic inflows, on the other hand, are driven by  
36 density gradients and stratification differences, often involving internal waves and subsurface transport  
37 mechanisms. MBIs transport large volumes of dense, oxygen-rich saline waters into deeper Baltic basins,  
38 replenishing oxygen levels in bottom waters and impacting both physical and ecological processes (Mohrholz,  
39 2018). The frequency, intensity, and impact of these inflow events are crucial for understanding the long-term  
40 environmental status of the Baltic Sea, influencing deep-water renewal and ecosystem dynamics (Reissmann et  
41 al., 2009).

42 Comprehensive observational datasets for the Southern Baltic Sea remain relatively scarce, particularly  
43 continuous, high-resolution Conductivity-Temperature-Depth (CTD) profiles spanning multiple decades (Feistel  
44 et al., 2008). **Hydrographic observations in the Baltic Sea are represented in long-standing international data  
45 compilations and infrastructures (e.g., ICES data archives, SeaDataNet, EMODnet, Copernicus Marine Service,  
46 and global repositories such as the World Ocean Database). However, many historical measurements are spatially  
47 heterogeneous or episodic, and a substantial fraction originates from fixed monitoring stations rather than repeated  
48 basin-scale sections. In contrast, the IOPAN program provides a rare, long-term, repeatedly sampled transect that  
49 consistently links the Arkona Basin, Bornholm Basin, Słupsk Furrow, and Gdańsk Basin, enabling coherent  
50 analysis of along-basin hydrographic structure and variability over nearly three decades.** While sporadic  
51 measurement campaigns and shorter-term datasets exist, long-term, systematic collections are limited, making it  
52 challenging to fully understand the variability and long-term trends in the region (Omstedt et al., 2014). This  
53 scarcity is especially pronounced within the Polish Exclusive Economic Zone (EEZ), where the availability of  
54 openly accessible, high-resolution CTD data is particularly limited. In contrast to the better-monitored central  
55 basins of the Baltic Sea—such as the Bornholm and Gotland Basins—data coverage in the Polish EEZ has been  
56 historically sparse and fragmented. Regular measurements in this area have often been conducted only a few times  
57 per year, and real-time or near-real-time data have not been readily available until the recent deployment of Argo  
58 floats (Walczowski et al., 2020). The lack of dense, long-term in situ CTD records hinders detailed analyses of  
59 vertical structure, stratification, oxygen dynamics, and long-term hydrographic shifts in this environmentally and  
60 economically important sector of the Baltic Sea. Furthermore, this data gap poses significant challenges to  
61 numerical modeling, operational oceanography, and marine environmental management.

62 Addressing this critical gap, this article introduces a unique, meticulously curated dataset comprising CTD profiles  
63 collected over 28 years (1997–2024) in the Southern Baltic Sea by the Observational Oceanography Laboratory  
64 of the Institute of Oceanology Polish Academy of Sciences (IOPAN), Physical Oceanography Department. The  
65 data, gathered systematically aboard the research vessel R/V Oceania, provide invaluable insights into the physical  
66 oceanographic processes shaping the local environment and their connection to broader climatic phenomena. Some  
67 of these data have already been used in previous publications on long-term changes in the southern Baltic Sea,  
68 including studies on temperature and salinity (Rak and Wieczorek, 2012), oxygen levels (Rak et al., 2020), the  
69 upper ocean mixing and stratification (Bulczak et al., 2024) and the sea energy (Rak et al., 2024), and inflow  
70 propagation (Rak, 2016). However, in this work, we make the full dataset publicly available and provide a  
71 comprehensive description of its processing and key features.

72 The significance of these measurements lies in their extensive temporal coverage and high spatial resolution, which  
73 enable comprehensive analyses of variability across a range of temporal scales—from seasonal to decadal—and  
74 spatial scales, from sub-mesoscale to basin-wide. Furthermore, this dataset serves as a vital resource for improving

75 numerical ocean modeling and validation efforts, contributing significantly to our understanding of both local  
76 marine dynamics and global climate-related processes (Gröger et al., 2021).

77

## 78 2. Study area and campaign design

79 The repeat hydrographic section follows the axis of the deep basins in the southern Baltic Sea, from the Arkona  
80 Basin through the Bornholm Basin and the Słupsk Furrow to the Gdańsk Basin. This section spans approximately  
81 280 nautical miles ( $\approx 519$  km), and the measurement time with the towed probe varies from 3 to 5 days, depending  
82 on weather conditions.

83 Although the monitoring program was originally designed to cover the full transect linking the Arkona Basin,  
84 Bornholm Basin, Słupsk Furrow, and Gdańsk Basin, not all cruises achieved complete spatial coverage. Weather  
85 conditions, ship-time constraints, and operational limitations occasionally resulted in partial transects or a reduced  
86 number of stations. Full-transect coverage was achieved most consistently prior to 2018. In subsequent years,  
87 reduced ship time, budget constraints, and operational limitations progressively curtailed the western reach of the  
88 section—first to the vicinity of the Bornholm Channel and ultimately to profiles within the Polish Exclusive  
89 Economic Zone, which remains the current operational limit. Nevertheless, the Gdańsk Basin and Słupsk Furrow  
90 were sampled during the majority of campaigns, ensuring continuity of the key hydrographic time series. Over the  
91 28-year period, the dataset therefore represents a quasi-regular repeated section rather than a perfectly uniform  
92 annual survey.

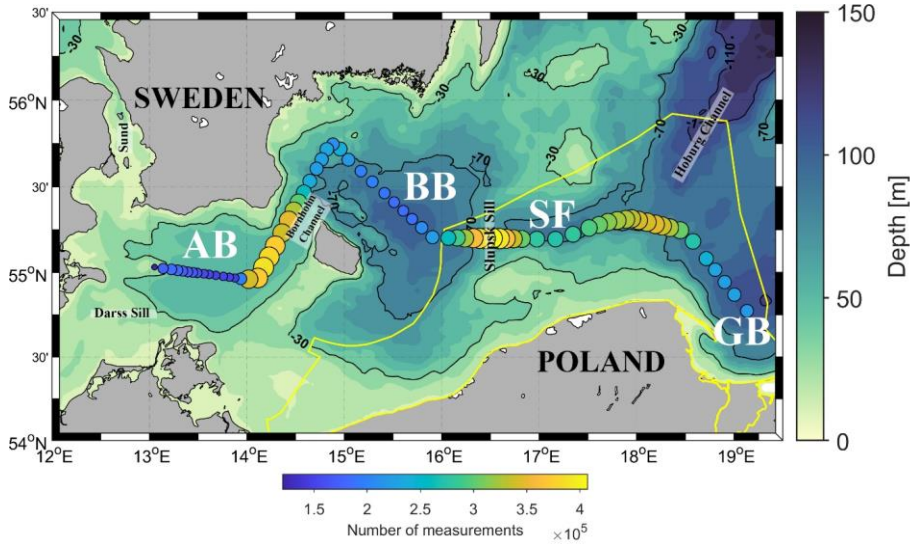
93 The transect evolved over time. Since the early 2000s, the core transect from the Bornholm Channel  
94 (Bornholmsgat) to the Gdańsk Basin has been performed in a highly repeatable manner. In contrast, the western  
95 segment across the Arkona Basin did not follow a single fixed track. Depending on logistics and weather  
96 conditions, the route varied between a more northerly pathway oriented toward the Sound and a more southerly  
97 pathway closer to the Darss Sill.

98 Over the 28-year period (Figure 1), sampling was designed to capture the pathways and transformation of  
99 North Sea inflow waters while maintaining consistent coverage within the Polish sector of the southern Baltic. As  
100 a result, data density is highest in the Bornholm Basin, the Słupsk Furrow and Słupsk Sill region, and the Gdańsk  
101 Basin, which together form the core observation corridor of the long-term monitoring. To quantify spatial  
102 coverage, we classified each cruise by its westernmost extent along the section (based on the westernmost station  
103 longitude). Approximately 31% of cruises reached the Arkona Basin, ~62% reached at least the Bornholm  
104 Channel, and ~80% reached at least the Bornholm Basin. This variability should be considered when interpreting  
105 basin-scale climatologies and the long-term statistics.

106

107

— sformatowano: Sprawdź pisownię i gramatykę



108  
 109 **Figure 1: Spatial distribution of CTD profiles collected during R/V Oceania cruises between 1997 and 2024 in the**  
 110 **southern Baltic Sea. The yellow line indicates the Polish Exclusive Economic Zone (EEZ). The labels AB, BB, SF and**  
 111 **GB denote the Arkona Basin, Bornholm Basin, Slupsk Furrow and Gdańsk Basin, respectively.**

112

### 113 3. Instruments and measurement modes

114 Hydrographic observations of IOPAN were conducted with several CTD systems (Table 1). Early operations used  
 115 a Guildline 87104 and an Idronaut OS316; the OS316 was soon complemented and largely superseded by the Sea-  
 116 Bird SBE49 FastCAT. All of these instruments were initially deployed in towed mode (underway profiling). Since  
 117 2020, vertical casts (stations) profiling has largely replaced towing, primarily with a Sea-Bird SBE19plus and,  
 118 more recently, an Idronaut OS316Plus. **No routine discrete water samples for salinity calibration were collected**  
 119 **during the majority of cruises. Salinity quality control relied on manufacturer calibration procedures, pre- and post-**  
 120 **cruise sensor checks, and internal consistency between temperature, conductivity, and density structure. Long-**  
 121 **term stability was additionally assessed through intercomparison between different CTD systems used over the**  
 122 **monitoring period and by verifying the consistency of deep-layer salinity signals during major inflow events.**

123

124 **Table 1: Overview of CTD instruments used by IOPAN for hydrographic observations in the southern Baltic Sea**  
 125 **between 1997 and 2024. The table lists the main devices and corresponding measurement types conducted during each**  
 126 **period.**

Year	CTD system	Measurement type
1997–1999	Guildline 87104	Towed
2000–2002	Idronaut OS316	Towed
2002–2003	Idronaut OS316; Sea-Bird SBE49	Towed

2004–2020	Sea-Bird SBE49; SBE19plus	Towed + vertical casts
2021–2023	Sea-Bird SBE19plus	vertical casts
2023–2024	Idronaut OS316Plus / Sea-Bird SBE19plus	Towed + vertical casts

127  
128 During towing, the CTD is mounted in a protective metal frame with an under-slung chain to minimize the risk of  
129 seabed contact. This configuration maintains a stable, near-horizontal probe orientation while providing  
130 mechanical protection (Figure 2). To produce a near-sinusoidal sampling pattern, the probe is cycled  
131 repeatedly between surface and bottom. At a towing speed of ~4 kn, this yields a horizontal resolution of ~200–  
132 500 m in typical water depths of 60–120 m. Towed data are acquired on both the downcast and upcast. Since 2020,  
133 vertical stations with a nominal along-track spacing ~5 nm have replaced towing. Owing to the probe’s mounting  
134 and its orientation relative to the direction of motion, only the downcast is retained for vertical (station)  
135 measurements. The nominal spacing of approximately 5 nautical miles between vertical stations was selected as a  
136 compromise between resolving mesoscale hydrographic structures and maintaining practical survey duration. In  
137 the southern Baltic basins, horizontal density and salinity gradients associated with inflow propagation, halocline  
138 tilt, and basin-scale circulation typically occur on spatial scales of 10–30 km. A 5 nm (~9 km) station interval  
139 therefore provides sufficient resolution to capture these gradients and the structure of the permanent halocline  
140 while allowing completion of the transect within available ship time and weather windows. This spacing has been  
141 maintained consistently over the monitoring period to ensure comparability of sections and long-term variability  
142 analyses.

— sformatowano: Sprawdź pisownię i gramatykę



144  
145 **Figure 2: CTD towed probe system used for the collection of data with Sea-Bird SBE49 (2002-2020)**

146  
147 Instrument choice for the towed platform was driven by high sample-rate capability and robust real-time telemetry.  
148 The Sea-Bird SBE19plus has been the primary shipboard profiling CTD on board R/V *Oceania*, whereas the  
149 Idronaut OS316Plus—initially used at stations—has more recently been integrated into a refurbished towed frame.  
150 A further advantage of the OS316Plus is its pass-through interface that allows additional auxiliary sensors (e.g.,

151 dissolved oxygen, turbidity) to be powered and telemetered over a single cable. Manufacturer accuracy  
 152 specifications for all instruments used in this program are summarized in Table 2.

153 **Table 2: Manufacturer specifications of conductivity-temperature-depth (CTD) profilers used by the Institute of**  
 154 **Oceanology, Polish Academy of Sciences (IOPAN) during long-term hydrographic monitoring in the southern Baltic**  
 155 **Sea.**

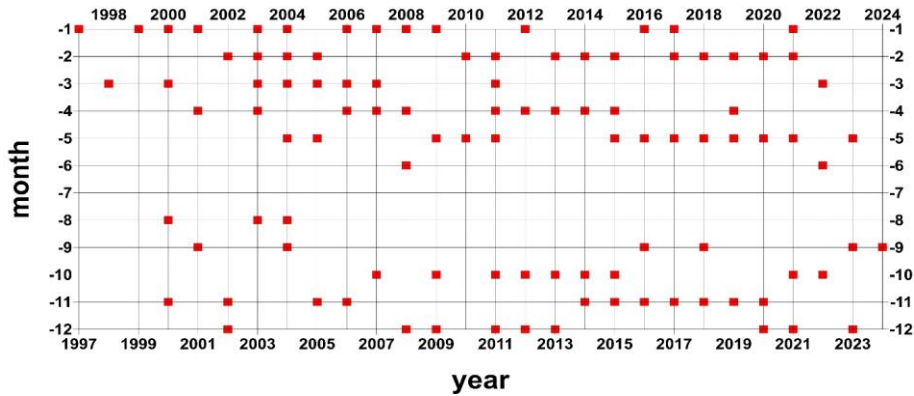
CTD system	Pressure Accuracy	Temperature Accuracy	Conductivity Accuracy	Sampling	Notes
<b>Guildline 87104</b>	(no public spec)	(no public spec)	(no public spec)	(no public spec)	Manufacturer specifications not publicly available.
<b>Idronaut OS316S</b>	±0.05 % FS (0–7000 dbar)	±0.003 °C	±0.0003 S m <sup>-1</sup>	4–16 Hz	Full-ocean-depth probe, pump-free, seven-ring quartz conductivity cell.
<b>Idronaut OS316Plus</b>	±0.05 % FS (standard); ±0.01 % FS	±0.002 °C	±0.0003 S m <sup>-1</sup>	12–20 Hz (real-time, typically 20 Hz)	Higher precision version, pump-free, 1500 dbar housing.
<b>Sea-Bird SBE49 FastCAT</b>	±0.1 % FS	±0.002 °C	±0.0003 S m <sup>-1</sup>	16 Hz	Autonomous CTD for vehicles/ROVs; high sample rate.
<b>Sea-Bird SBE19plus / V2</b>	±0.1 % FS (strain-gauge) / ±0.02 % FS (quartz)	~±0.005 °C	~±0.0005 S m <sup>-1</sup>	4–6 Hz	Widely used profiling CTD, V2 offers quartz pressure option.

156

#### 157 4. Dataset and methods

158 Observational data utilized in this study were gathered during research voyages of the Institute of Oceanology of  
 159 the Polish Academy of Sciences' vessel, R/V Oceania. These data originated from the Southern Baltic Sea,  
 160 spanning the period between 1997 and 2024 (Figure 3). Approximately four surveys were conducted  
 161 annually, with the observational program designed to cover the full repeat section linking the Arkona Basin,  
 162 Bornholm Basin, Stupsk Furrow, and Gdańsk Basin. In practice, the number of surveys per year varied (typically  
 163 2–5) depending on ship availability, weather, and operational constraints, and not all cruises achieved full spatial  
 164 coverage (see Section 2). Owing to the engagement of R/V Oceania in the Arctic research, the period from June  
 165 to August is the least represented in the dataset.

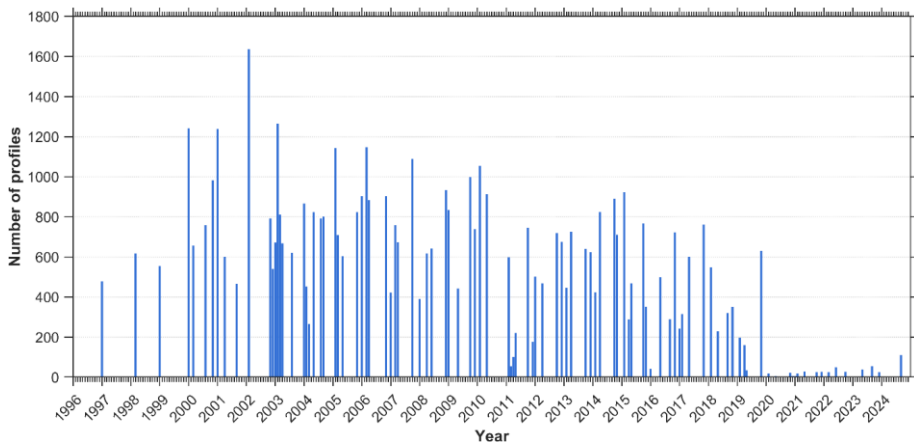
166 The temporal sampling is therefore not uniform over the 28-year period. Sampling frequency was the highest in  
 167 the early and mid-2000s, when intensive towed surveys provided dense profile coverage, and decreased after 2020  
 168 due to the loss of the SBE49 towed system, reduced ship time, and logistical constraints. As a result, the dataset  
 169 contains interannual variability in the number of cruises and profiles. This heterogeneity should be considered  
 170 when applying statistical methods that assume regular sampling (e.g., long-term linear trend estimation or evenly  
 171 spaced climatologies). The dataset is, however, fully suitable for analyses focused on vertical structure, water-  
 172 mass variability, stratification, and episodic processes such as inflow and ventilation events, which depend  
 173 primarily on profile-scale resolution rather than uniform temporal spacing.



174  
 175 **Figure 3: Time distribution (1997–2024) of R/V Oceania CTD cruises conducted by the Observational Oceanography**  
 176 **Laboratory, Institute of Oceanology PAN.**

177 In total, from 1997 to 2024, 96 hydrographic voyages were conducted, during which 55032 measurement profiles  
 178 were recorded (Figure 4). The annual profile counts show strong interannual variability with a clear  
 179 maximum in the early–mid 2000s, when intensive towed CTD surveys routinely yielded several hundred to >1,000  
 180 profiles per year. From the late 2000s into the 2010s the effort gradually declined, reflecting reduced sea time and  
 181 a growing share of discrete station work. A sharp drop is evident after 2019, consistent with the loss of the SBE49  
 182 towed system in May 2020 and COVID-19 operational constraints; only sparse profiles were collected in 2020–  
 183 2024. Overall, the variability primarily reflects instrument availability, cruise logistics, and weather, rather than  
 184 changes in processing or quality control.

— sformatowano: Sprawdź pisownię i gramatykę



186  
 187 **Figure 4: Distribution of CTD profiles conducted by IOPAN along the main monitoring transect in the southern Baltic**  
 188 **Sea.**

189  
 190 Towed measurements made with the Guildline 87104, Idronaut OS316, and Sea-Bird SBE49 typically store a  
 191 single geographic position and timestamp at the beginning of each profile. Because the probe trails behind the

192 vessel on a cable, the actual sampling position deviates from the ship's GPS location. The horizontal offset  
193 increases with depth and cable length. A simple geometric upper bound assuming a large cable angle suggests that  
194 near-bottom samples could, in extreme cases, be displaced by up to approximately three times the local water  
195 depth (e.g., ~300 m at 100 m depth). In practice, however, actual offsets are substantially smaller and remain  
196 negligible relative to the mesoscale and basin-scale variability resolved by the section.

197 For vertical (station) profiles, positional uncertainty is much smaller and arises primarily from vessel drift during  
198 the cast. In the southern Baltic, station drift is typically modest; when present, it reflects a combination of wind  
199 forcing and local currents during the cast, but remains small relative to the nominal station spacing. In systems  
200 such as the Idronaut OS316Plus, each sample is associated with a geographic position; however, this corresponds  
201 to the ship's GPS location rather than the exact sensor position in the water column. Consequently, a small  
202 horizontal offset remains, but it is minor compared to the horizontal scales resolved by the nominal station spacing.

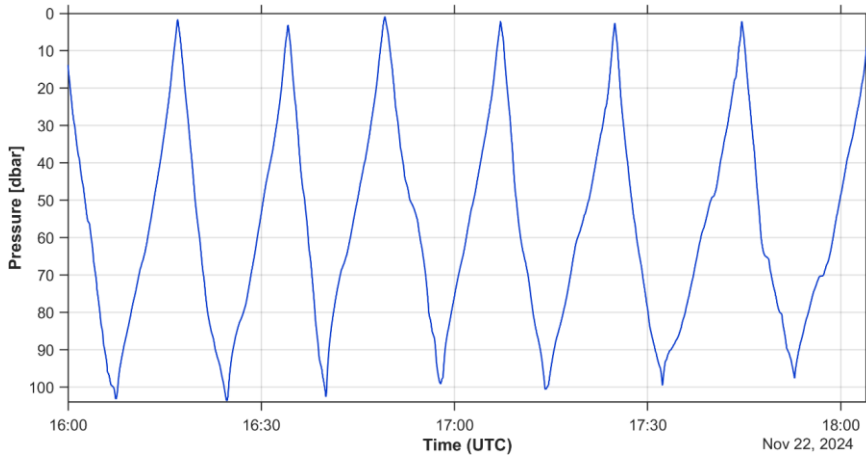
203 As illustrated in [Figure 5](#) for the towed measurements, the descent rate is not uniform: it varies when  
204 crossing the pycnocline and with irregular ship motion. Additionally, winch speed is routinely reduced near the  
205 surface and close to the seabed for safety reasons, further modulating sampling speed.

206  
207 From 1997 to 2020, towed operations were routine. On 20 May 2020 the towed system carrying the Sea-Bird  
208 SBE49 was lost; since then, measurements have been conducted predominantly as vertical station casts, with  
209 limited towing resumed in 2023–2024 using a refurbished frame. In the post-2020 period, towing is applied  
210 selectively due to weather constraints and reduced ship time (typically ~7-day cruises vs ~14 days in earlier  
211 intensive periods, e.g., around 2003), and is therefore combined with a reduced set of station casts.

212 The number of cruises decreased after 2020, leading to a temporal discontinuity in sampling frequency.  
213 Accordingly, analyses that require regular annual sampling, such as precise decadal trend estimation, should be  
214 interpreted with caution. However, the dataset remains fully suitable for studies of vertical structure, stratification,  
215 water-mass variability, and episodic events (e.g., inflows and ventilation), which depend primarily on profile-scale  
216 resolution. Complementary observations from Argo floats and global data archives provide additional regional  
217 context during periods of reduced ship-based sampling, although they generally lack the spatial focus and  
218 repeatability of the IOPAN section.

219  
220  
221

— sformatowano: Sprawdź pisownię i gramatykę



222  
 223 **Figure 5: Example of a typical continuous CTD probe trajectory in the water column during towed measurements.**

224

225 **4.1 Instrument calibration and uncertainty budget**

226 All Sea-Bird sensors used in this dataset (SBE 49 FastCAT, Sea-Bird SBE19plus / V2) were regularly returned to  
 227 Sea-Bird GmbH (Kempten, Germany) for servicing and post-cruise calibration, typically every 1–3 years,  
 228 depending on instrument usage and cruise schedules. Service reports document routine post-cruise calibration of  
 229 temperature and conductivity sensors, calibration of pressure sensors, firmware updates and full system checks for  
 230 the SBE 49 FastCAT and associated pump and conductivity modules.

231 For the most frequently used CTD on the towed system (Sea-Bird SBE 49 FastCAT), the latest post-cruise  
 232 calibration performed in March 2018 yielded extremely small residuals relative to laboratory standards.  
 233 Temperature calibration over the range 1–32.5 °C showed residuals within  $\pm 0.0001$  °C, i.e. more than an order of  
 234 magnitude smaller than the nominal manufacturer accuracy.

235 Conductivity calibration residuals were on the order of  $10^{-4}$  S  $m^{-1}$  across the full range of bath salinities, i.e.  
 236 negligible compared to the nominal conductivity accuracy.

237 Pressure calibration for the 870-psia ( $\approx 600$  dbar) pressure sensor showed residuals within  $\pm 0.01$  % of full scale,  
 238 effectively at the limit of the calibration procedure.

239 Based on manufacturer specifications and these post-cruise calibration results, we adopt conservative instrumental  
 240 uncertainties of  $\pm 0.005$  °C for temperature,  $\pm 0.01$  in practical salinity and  $\pm 0.5$  dbar for pressure for individual 1-  
 241 dbar binned measurements from Sea-Bird CTDs. These values are larger than the formal calibration residuals, but  
 242 they account for potential long-term sensor drift between service intervals and any residual biases introduced by  
 243 data processing (vertical binning, median filtering) and deployment configuration (e.g. slight lags due to pump  
 244 response and flow through the conductivity cell). For other CTD models used earlier in the time series (Guildline  
 245 87104, Idronaut OS316), we adopt comparable or slightly larger uncertainties consistent with manufacturer  
 246 specifications and our internal cross-comparisons (Table 3). The Idronaut OS316Plus was factory-calibrated at  
 247 Idronaut (24 Nov 2025). Although the dataset analysed here ends in 2024, we report the most recent factory  
 248 calibration to document instrument performance and to motivate the conservative uncertainties adopted for the

249 processed products. Calibration residuals were within  $\pm 0.0011$  °C for temperature and  $\pm 0.0039$  mS/cm for  
 250 conductivity. For consistency with the long-term record and to account for drift between service intervals and  
 251 processing effects, we adopt conservative uncertainties of  $\pm 0.005$  °C,  $\pm 0.01$  PSU, and  $\pm 1$  dbar for 1-dbar binned  
 252 products.

253

254 **Table 3: Overview of the main CTD instruments used in the dataset and the conservative instrumental uncertainties**  
 255 **adopted for temperature, practical salinity (PSS-78; reported here in PSU) and pressure.**

Period	Main CTD model	Calibration interval	Temperature uncertainty (°C)	Salinity uncertainty (PSU)	Pressure uncertainty (dbar)
1997–1999	Guildline 87104	No data	No data	No data	No data
2000–2003	Idronaut OS316	every 3 years	$\pm 0.01$	$\pm 0.02$	$\pm 1$
2004–2020	SBE 49 / SBE19plus	every 1–2 years	$\pm 0.005$	$\pm 0.01$	$\pm 0.5$
2023–2024	Idronaut OS316Plus	every 2 years	$\pm 0.005$	$\pm 0.01$	$\pm 1$

256

257 In addition to instrumental uncertainties, there is a finite spatial representativeness error associated with towed  
 258 sections. During towing, the CTD is pulled astern and may therefore be horizontally displaced from the ship’s GPS  
 259 position. Simple geometric considerations show that an extreme upper bound of three times the local depth would  
 260 require the tow cable to be almost horizontal, which is unrealistic for our operating conditions (towing speeds of  
 261  $\approx 4$  kn and depths of 60–100 m). In practice, observed cable angles correspond to horizontal offsets of the order  
 262 of 0.3–0.8 times the local depth; for the error budget we therefore adopt the local depth as a conservative upper  
 263 limit on horizontal position uncertainty ( $\approx 100$  m at 100 m depth), while typical offsets are likely closer to 0.5  
 264 times the depth. We therefore recommend that the dataset be used primarily for basin-scale and mesoscale  
 265 analyses, rather than for resolving fine-scale ( $< O(100$  m)) frontal structures, where unresolved horizontal offsets  
 266 may become non-negligible.

## 267 5. Quality check and postprocessing of CTD data

268 The quality control (QC) and postprocessing procedures applied to the CTD data collected by IOPAN are essential  
 269 for ensuring the scientific value, internal consistency, and long-term usability of the dataset. Raw data were  
 270 recorded using several CTD systems operated over the multi-decade period and were calibrated according to  
 271 manufacturer recommendations. **Thermal-lag (temperature–conductivity misalignment) effects were addressed**  
 272 **during standard instrument preprocessing prior to salinity computation. Subsequent pressure sorting, 1-dbar**  
 273 **binning, and median filtering further reduce residual high-frequency noise while preserving mesoscale gradients.**  
 274 Postprocessing starts with an automated MATLAB routine that imports CNV/TXT files and parses station  
 275 metadata (date/time and geographic coordinates). Raw samples are first screened for common acquisition artefacts:

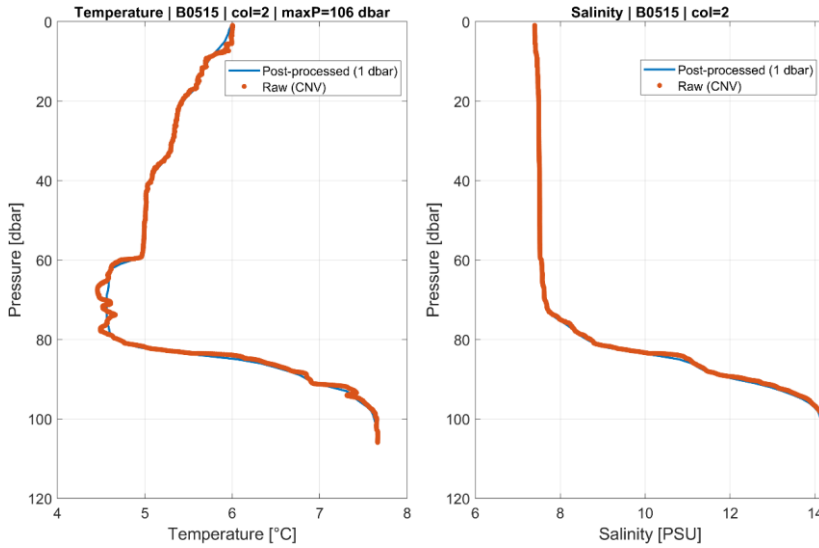
276 records with negative pressure ( $p < 0$  dbar) are removed, and instrument fill values (e.g.,  $-9.990 \times 10^{-29}$ ) are  
277 converted to NaN. Each cast is then sorted by pressure, repeated pressure levels are consolidated by averaging,  
278 and the profile is standardized onto a uniform vertical axis (0–199 dbar,  $\Delta p = 1$  dbar) using local averaging within  
279 a  $\pm 1$  dbar window around each target level. Temperature and salinity are denoised using a running median filter  
280 (movmedian, window size typically 20 samples, omitting NaNs). Profiles with missing or invalid metadata are  
281 excluded by masking casts where longitude/latitude/time are equal to 0 or NaN. For the gridded processing stream,  
282 navigation is additionally quality-checked using broad domain limits (lon 13–22°E, lat 54.2–58°N) and a despiking  
283 rule that flags positions deviating by more than  $0.1^\circ$  from a 5-point running median; flagged lon/lat/time values  
284 are propagated as a common mask across variables.

285 Hydrographic variables are further checked for physically implausible values and unstable segments. Salinity is  
286 constrained to a plausible range (7.2–21), with values outside this range set to NaN. **The adopted salinity range is  
287 based on the long-term hydrographic characteristics of the southern Baltic Sea. These limits are consistent with  
288 regional climatological conditions and historical monitoring data. The vast majority of observations throughout  
289 the 28-year record fall within this interval. Values outside the adopted range therefore represent clear outliers  
290 attributable to measurement artefacts or processing errors rather than physically plausible hydrographic conditions.  
291 A single conservative salinity range was applied uniformly across all basins as part of the automated QC pipeline,  
292 to avoid spatially dependent filtering and ensure consistent treatment of all profiles.**

293 **A static-stability check based on TEOS-10 density was applied. Adjacent levels implying any density inversion  
294 ( $\Delta \rho < 0$  kg m<sup>-3</sup>) were flagged as unstable, and the corresponding salinity values were set to NaN.** Profiles are  
295 truncated below the first occurrence of  $\geq 5$  consecutive NaNs in salinity, and casts exhibiting an abrupt salinity  
296 decrease larger than 0.01 between adjacent levels are terminated from that depth downward. For the gridded  
297 product, an additional optional vertical smoothing step is applied using a moving mean (smoothdata, window 10)  
298 to reduce residual small-scale noise while retaining vertical gradients.

299 After automated QC and postprocessing, profiles are aggregated into structured arrays, enabling downstream  
300 climatological and statistical analyses. The processed data are routinely visualized to identify potential outliers  
301 and systematic artefacts, and a manual review complements the automated steps, particularly for casts affected by  
302 strong ship motion or transient sensor behaviour. To illustrate the effect of our pipeline, Figure 6 contrasts a raw  
303 cast with its post-processed counterpart for cruise B0515. This cast was selected as a stress-test case with  
304 pronounced motion/sensor transients near the halocline. Residual small-scale noise visible in the raw data is only  
305 lightly attenuated by design: our post-processing is intentionally conservative to preserve mesoscale gradients and  
306 avoid over-smoothing that could bias stratification metrics.

307



308  
 309 **Figure 6: Example of a raw CTD profile and the same profile after post-processing. Raw CNV samples (dots) and the**  
 310 **1-dbar product (solid line) are shown for temperature (°C) and salinity (PSU); pressure increases downward (dbar).**

311  
 312

### 313 6. Data structure and export

314 The dataset is delivered in two interoperable formats. First, as a single MATLAB container in which each cruise  
 315 is stored as a separate field of the top-level struct IOPAN. Cruise fields follow the BMMYY convention (B –  
 316 Baltic; MM – month; YY – year; e.g., B0523 for May 2023) and contain gridded, column-oriented hydrographic  
 317 profile matrices together with a shared vertical coordinate. Second, the same cruise-wise products are exported as  
 318 a collection of per-cruise NetCDF files (IOPAN\_BMMYY.nc) compliant with the CF-1.8 conventions and the  
 319 discrete sampling geometry (DSG) profile representation, with depth × profile hydrographic variables and profile-  
 320 wise (1-D) geolocation and time coordinates.

321  
 322 MATLAB (IOPAN\_Baltic.mat)

323 For each cruise:

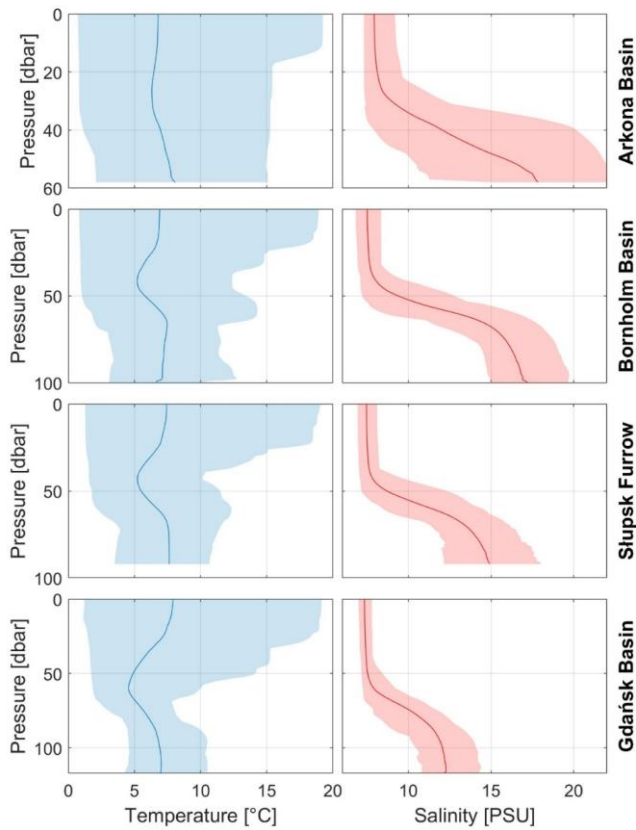
- 324 • Pressure, Temperature, Salinity: size N×M, where rows are 1-dbar levels and columns are individual profiles.
- 325 • Pressure\_string: size N×1, the common vertical grid (e.g., 0:1:199 dbar).
- 326 • Time (MATLAB datenum), Longitude, Latitude: stored as size N×M for convenience and co-registration with  
 327 the hydrographic matrices; within each profile (column) these values are constant with depth (i.e., they represent  
 328 station-level metadata repeated along the vertical). Timestamps represent MATLAB serial days (fractional part =  
 329 time of day) and should be interpreted as UTC unless stated otherwise.

330  
 331 NetCDF (IOPAN\_BMMYY.nc)

332 The NetCDF files use a compact CF-DSG layout in which:  
333 • Hydrographic variables are stored on a common pressure grid (dbar) as 2-D arrays with dimensions (pressure,  
334 profile), with 1-D coordinates lon(profile), lat(profile), and time(profile).  
335 • Coordinates lon(profile) and lat(profile) are stored as 1-D profile-wise variables.  
336 • Time is provided as a 1-D CF-compliant coordinate time(profile) (e.g., seconds since 1970-01-01 00:00:00 UTC,  
337 calendar = gregorian).  
338 During export, the station-level time and position are obtained from the MATLAB N×M matrices by extracting a  
339 representative value per profile (e.g., the first finite value in each column).  
340 A metadata block accompanies the cruise fields and documents units, creation timestamp, ownership and contact  
341 point. Missing or filtered values are encoded as NaN in MATLAB and as \_FillValue in NetCDF; pruning during  
342 processing removes empty profiles (all-NaN columns) and ensures consistent dimensions within each cruise. The  
343 processing and export workflow is implemented in the MATLAB scripts build\_IOPAN\_from\_CNV\_TXT.m and  
344 write\_IOPAN\_to\_netcdf.m (Zenodo, <https://doi.org/10.5281/zenodo.17814769>).

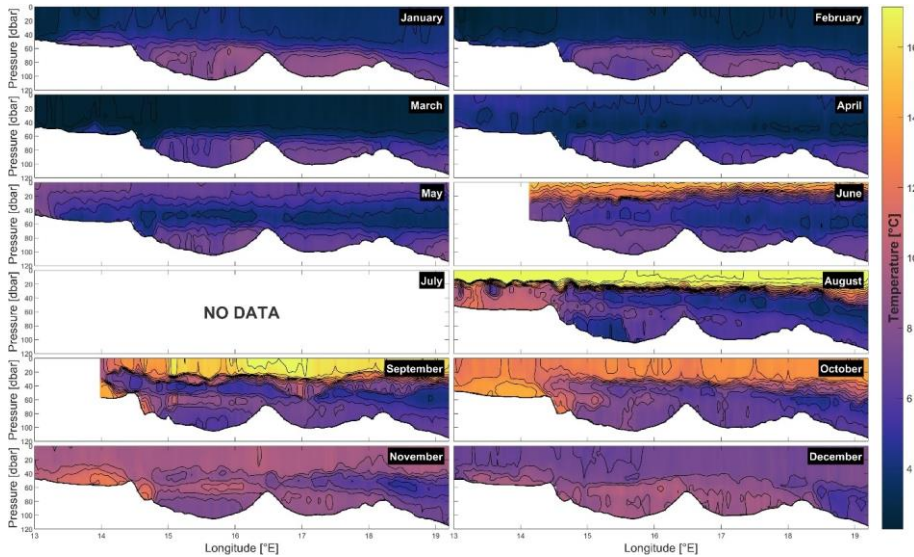
#### 345 **7. Basin-scale hydrographic structure and variability**

346 Basin-scale vertical structure along the repeat transect is summarized in Figure 7. In all four basins, the upper ~40–  
347 60 dbar are dominated by seasonally varying, relatively fresh surface waters, as reflected in the broad temperature  
348 envelope and modest salinity range. Below the seasonal thermocline, temperature variability is much reduced,  
349 while salinity exhibits a pronounced step-like increase across the permanent halocline. **Below ~50 dbar, salinity**  
350 **variability increases markedly compared with the upper layer. This depth range corresponds to the permanent**  
351 **halocline that separates the seasonally mixed brackish surface waters from deeper, more saline North Sea–derived**  
352 **water masses. Variability at depth is therefore governed by episodic inflow events, lateral spreading of saline**  
353 **intrusions, and isopycnal mixing, while the upper layer is more frequently homogenized by wind-driven and**  
354 **seasonal mixing processes. The mean halocline depth and deep salinity systematically change along the section:**  
355 **in the shallow Arkona Basin stratification is generally confined to the upper water column; however, during inflow**  
356 **periods this basin often contains some of the highest salinities observed along the section and can exhibit a**  
357 **pronounced halocline extending from ~30 dbar to the bottom. Farther east, the Bornholm Basin and Slupsk Furrow**  
358 **display strong, well-defined haloclines overlying more saline deep waters. Toward the Gdańsk Basin, deep**  
359 **salinities decrease and the halocline shoals slightly, consistent with progressive dilution and mixing of North Sea**  
360 **inflow waters along their downstream pathway. The shaded ranges highlight that, despite substantial interannual**  
361 **and event-scale variability, the basic vertical structure and along-transect contrasts between basins are robust**  
362 **features of the 28-year record.**  
363



364  
 365 **Figure 7: Basin-mean vertical profiles of temperature and salinity in the Arkona Basin, Bornholm Basin, Slupsk Furrow**  
 366 **and Gdańsk Basin derived from all CTD casts collected along the repeat section between 1997 and 2024. Solid lines**  
 367 **indicate the multi-year mean and shaded envelopes the full range (min–max) across all cruises.**

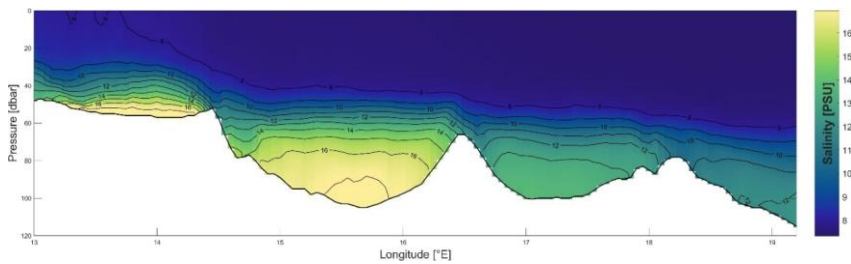
368  
 369 Monthly mean temperature sections (January–December) along the repeat Baltic transect are shown in Figure 8.  
 370 The 12-panel climatology highlights the pronounced seasonal cycle of the upper water column, with winter cooling  
 371 and a deep, relatively homogeneous mixed layer followed by spring onset of stratification, summer surface  
 372 warming and development of a shallow thermocline, and an autumnal erosion of stratification. A persistent  
 373 dichothermal (cold intermediate) layer is visible from approximately April through November, reflecting winter-  
 374 cooled water retained below the seasonal thermocline while the surface layer warms. Along-transect differences  
 375 reflect the changing basin geometry and hydrographic regime from the Arkona Basin through the Bornholm Basin  
 376 and Slupsk Furrow toward the Gdańsk Basin, and the month-to-month variability in deeper layers suggests that  
 377 advection plays a key role in shaping the subsurface temperature field along the monitoring section.  
 378



379  
 380 **Figure 8: Monthly mean temperature sections (January–December) along the Baltic transect as a function of longitude**  
 381 **(°E) and pressure (dbar).**

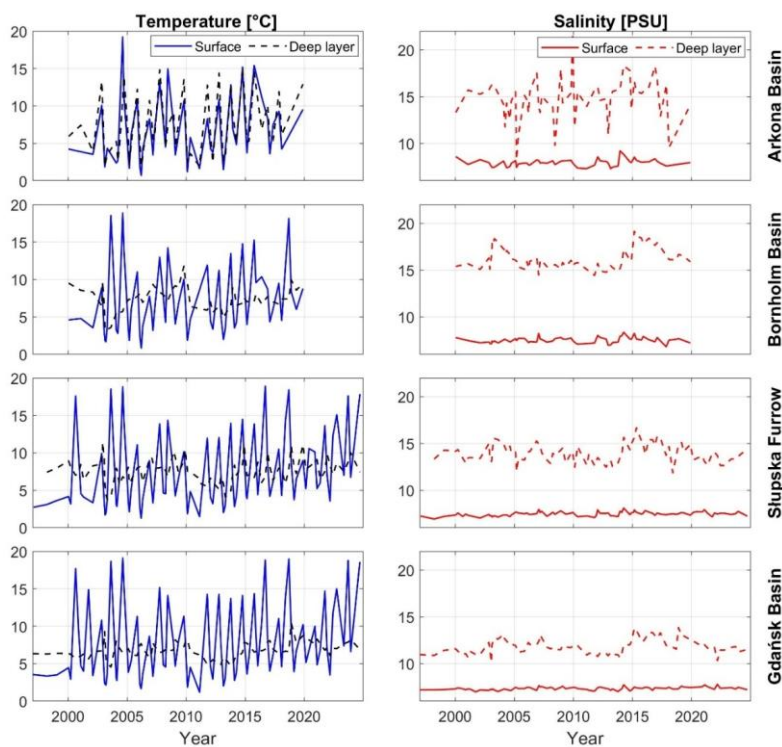
382  
 383 In contrast to temperature, salinity does not exhibit a pronounced seasonal cycle. Surface salinity variability is  
 384 mainly influenced by episodic freshwater input, vertical mixing, and horizontal advection, while deeper salinity  
 385 variability reflects irregular advective and mixing processes rather than seasonally phase-locked forcing. Because  
 386 salinity variability is dominated by these irregular and spatially structured processes rather than a repeatable annual  
 387 cycle, its large-scale characteristics are more clearly represented by the multi-year mean section. Figure 9 shows  
 388 the multi-year mean salinity section along the repeat southern Baltic transect. The upper ~40–60 dbar is dominated  
 389 by relatively fresh surface waters, while a distinct step-like increase in salinity below marks the permanent  
 390 halocline; this halocline is most pronounced over the Bornholm Basin and Stupsk Furrow, which also host the  
 391 highest salinities in deeper layers. Farther east toward the Gdańsk Basin, deep salinity decreases and the halocline  
 392 structure changes along the section, reflecting the along-transect hydrographic contrasts and downstream  
 393 modification of more saline waters.

394



395  
 396 **Figure 9: Mean salinity (1997–2024) section along the repeat Baltic transect, shown as a function of longitude (°E) and**  
 397 **pressure (dbar).**

398 Complementary basin-mean time series of layer-averaged temperature and salinity (Figure 10) illustrate how this  
 399 vertical structure evolves in time. The 0–10 dbar surface layer is characterized by large interannual variability in  
 400 temperature and relatively modest changes in salinity, reflecting the combined influence of atmospheric forcing,  
 401 riverine input, and local mixing. In contrast, the bottom layer (defined consistently as the interval from 20 dbar  
 402 above the seabed down to the bottom) varies more episodically, with pronounced salinity and temperature  
 403 anomalies associated with inflow-driven ventilation events and subsequent stagnation periods. Along the transect,  
 404 deep-layer signals are particularly pronounced in the Arkona Basin and in the deeper Bornholm Basin and Słupsk  
 405 Furrow, and become progressively attenuated toward the Gdańsk Basin, in line with the downstream  
 406 transformation of dense inflow waters inferred from the vertical structure in Figure 7. **The comparatively strong  
 407 deep-layer signals observed in the Arkona Basin reflect its position as the first basin reached by North Sea inflow  
 408 waters entering the Baltic. These newly arrived waters retain high salinity and oxygen content and have undergone  
 409 limited dilution or mixing, leading to pronounced anomalies. Farther east, in the Bornholm Basin and Słupsk  
 410 Furrow, the same inflow waters are progressively modified through mixing and entrainment (Bulczak and Rak,  
 411 2026), which reduces the amplitude of deep-layer signals.**  
 412



413  
 414 **Figure 10: Basin-mean time series of layer-averaged temperature (left) and salinity (right) in the Arkona, Bornholm,**  
 415 **Słupsk Furrow and Gdańsk basins for 1997–2024. Solid lines show the surface layer (0–10 dbar), while dashed lines**  
 416 **show a bottom layer defined uniformly from 20 dbar above the bottom down to the bottom in each basin.**

417 **8. Conclusion**

418  
419 We present a unique, quality-controlled CTD dataset spanning 1997–2024, assembled along a repeat section from  
420 the Arkona Basin through the Bornholm Basin and Słupsk Furrow to the Gdańsk Basin. In total, 96 cruises and  
421 55,032 profiles were collected, providing rare temporal continuity and along-track resolution for the southern  
422 Baltic Sea.

423 The observing system evolved from high-rate towed profiling to a hybrid approach that, since 2020, also includes  
424 vertical station casts with a nominal  $\leq 5$  nm spacing. Instrumentation progressed from Guildline 87104 and  
425 Idronaut OS316 to Sea-Bird SBE49 and SBE19plus, and most recently Idronaut OS316Plus—choices driven by  
426 sampling-rate capability and robust telemetry. Together, these modes and sensors yield horizontal scales of ~200–  
427 500 m at ~4 kn in 60–120 m depths and enable both down- and up-cast sampling in tow.

428 A consistent processing chain—standardized parsing of CNV/TXT, robust time/position handling, binning to 1  
429 dbar, median filtering, automated geolocation QC, and pruning of incomplete casts—ensures inter-comparability  
430 through time and across instruments. The final distribution package (IOPAN\_Baltic.mat) provides cruise-wise  
431 fields (BMMYY) with 1-dbar vertical grids, co-registered P–T–S matrices, and MATLAB serial-day time stamps  
432 (UTC), ready for analysis and conversion.

433 We explicitly acknowledge limitations that inform interpretation: reduced summer coverage due to Arctic  
434 commitments; tow-induced horizontal uncertainty comparable to the local depth (with typical offsets  $\approx 0.5 \times$  depth;  
435 see Section Instrument calibration and uncertainty budget); and a marked post-2020 decline in sampling linked to  
436 the loss of the SBE49 towed system (May 2020) and COVID-19 constraints. These variations predominantly  
437 reflect instrument availability, logistics, and weather rather than changes in QC or processing.

438 Despite these constraints, the dataset fills a long-standing observational gap in the Polish EEZ, where long, high-  
439 resolution CTD time series have been scarce, thereby strengthening model validation, reanalysis, and process  
440 studies of stratification, mixing, and inflow-driven ventilation along hydraulic controls. The section also serves as  
441 a reference line for quality control and validation of Baltic Argo float profiles and other autonomous observations,  
442 anchoring their measurements in a well-characterized hydrographic framework.

443 By making the full resource publicly available in both MATLAB and CF-compliant NetCDF formats, with  
444 transparent methods and structure, we provide an immediate foundation for multi-scale studies—from seasonal to  
445 decadal variability in temperature and salinity to the propagation and transformation of North Sea inflows—and  
446 for data assimilation in regional models. Continued observations along this established transect, ideally with  
447 renewed high-rate towed capability and routine auxiliary sensors (e.g., dissolved oxygen, turbidity) leveraging the  
448 OS316Plus pass-through interface, will be essential for tracking ongoing hydrographic change and supporting  
449 evidence-based management in the Baltic Sea.

450

451  
452 **Code availability**  
453 The MATLAB scripts used to build the processed IOPAN structure (Rak, 2025) from raw exports and to generate  
454 the CF-1.8 NetCDF products (build\_IOPAN\_from\_CNV\_TXT.m and write\_IOPAN\_to\_netcdf.m) are archived  
455 on Zenodo at <https://doi.org/10.5281/zenodo.17814769>.

456  
457 **Data availability**  
458 The full dataset (Rak, 2025) is available from <https://doi.org/10.48457/IOPAN.2025.531> in two formats: a single  
459 MATLAB file (IOPAN\_Baltic.mat) containing all cruises as the IOPAN struct, and a collection of per-cruise, CF-  
460 1.8-compliant NetCDF files (IOPAN\_BMMYY.nc, one file per cruise). Both formats provide the same gridded  
461 hydrographic fields and associated metadata, enabling straightforward use in MATLAB, Python and other  
462 common analysis environments.

463  
464 **Author contribution**  
465 DR coordinated the compilation of the IOPAN CTD dataset, designed the processing and quality-control  
466 workflow, processed and quality-controlled the data, developed the MATLAB processing and NetCDF export  
467 scripts, and prepared the figures and the initial manuscript draft. All authors contributed to CTD data acquisition  
468 during the cruises, participated in discussions on data interpretation and quality assessment, reviewed the  
469 manuscript, and approved the final version.

470  
471 **Competing interests**  
472 The authors declare that they have no conflict of interest.

473 **Acknowledgements**  
474 We gratefully acknowledge the late Prof. dr hab. Jan Piechura, co-author of this study, for his invaluable  
475 contribution to the collection of the hydrographic data used here. We also thank the crew of r/v Oceania for their  
476 long-term support during the field campaigns.

477 **Funding**  
478 This publication was supported by the following project: Argo-Poland, funded by the Polish Minister of Education  
479 and Science [grant number 2022/WK/04].

480

481 **References**

- 482
- 483 Bulczak, A. I., Nowak, K., Jakacki, J., Muzyka, M., Rak, D., & Walczowski, W. (2024). Seasonal variability and  
484 long-term winter shoaling of the upper mixed layer in the southern Baltic Sea. *Continental Shelf Research*, 276,  
485 105232. <https://doi.org/10.1016/j.csr.2024.105232>
- 486 **Bulczak A.I and Rak D (2026). Propagation and mixing of the 2023/24 inflow: impacts on stratification  
487 and deep-water ventilation in the Southern Baltic Sea. *Front. Mar. Sci.* 13:1629491.  
488 <https://doi.org/10.3389/fmars.2026.1629491>**
- 489 Burchard, H., Lass, H.-U., Mohrholz, V., Umlauf, L., Sellschopp, J., Fiekas, V., Bolding, K., & Arneborg, L.  
490 (2005). Dynamics of medium-intensity dense water plumes in the Arkona Basin, Western Baltic Sea. *Ocean  
491 Dynamics*, 55(5), 391–402. <https://doi.org/10.1007/s10236-005-0025-2>
- 492 Feistel, R., Nausch, G., & Wasmund, N. (Eds.). (2008). *State and Evolution of the Baltic Sea, 1952–2005: A  
493 detailed 50-year survey of meteorology and climate, physics, chemistry, biology, and marine environment.*  
494 Wiley.
- 495 Fischer, H., & Matthäus, W. (1996). The importance of the Drogden Sill in the Sound for major Baltic inflows.  
496 *Journal of Marine Systems*, 9(3–4), 137–157. [https://doi.org/10.1016/S0924-7963\(96\)00046-2](https://doi.org/10.1016/S0924-7963(96)00046-2)
- 497 Gröger, M., Dieterich, C., Haapala, J., Ho-Hagemann, H. T. M., Hagemann, S., Jakacki, J., May, W., Meier, H.  
498 E. M., Miller, P. A., Rutgersson, A., and Wu, L. (2021). Coupled regional Earth system modeling in the Baltic  
499 Sea region. *Earth System Dynamics*, 12, 939–973. <https://doi.org/10.5194/esd-12-939-2021>
- 500 Leppäranta, M., & Myrberg, K. (2009). *Physical Oceanography of the Baltic Sea*. Springer.  
501 <https://doi.org/10.1007/978-3-540-79703-6>
- 502 Matthäus, W., & Franck, H. (1992). Characteristics of major Baltic inflows—A statistical analysis. *Continental  
503 Shelf Research*, 12(12), 1375–1400. [https://doi.org/10.1016/0278-4343\(92\)90060-W](https://doi.org/10.1016/0278-4343(92)90060-W)
- 504 Mohrholz, V., Naumann, M., Nausch, G., Krüger, S., & Gräwe, U. (2015). Fresh oxygen for the Baltic Sea—An  
505 exceptional saline inflow after a decade of stagnation. *Journal of Marine Systems*, 148, 152–166.  
506 <https://doi.org/10.1016/j.jmarsys.2015.03.005>
- 507 Mohrholz, V. (2018). Major Baltic inflow statistics—Revised. *Frontiers in Marine Science*, 5, 384.  
508 <https://doi.org/10.3389/fmars.2018.00384>
- 509 Omstedt, A., Elken, J., Lehmann, A., Leppäranta, M., Meier, H. E. M., Myrberg, K., & Rutgersson, A. (2014).  
510 Progress in physical oceanography of the Baltic Sea during the 2003–2014 period. *Progress in Oceanography*,  
511 128, 139–171. <https://doi.org/10.1016/j.pocean.2014.08.010>
- 512 Rak, D. (2016). The inflow in the Baltic Proper as recorded in January–February 2015. *Oceanologia*, 58(3), 241–  
513 247. <https://doi.org/10.1016/j.oceano.2016.04.001>
- 514 Rak, D. (2025). IOPAN Baltic CTD processing and CF-1.8 NetCDF export (MATLAB) (1.0.0). Zenodo.  
515 <https://doi.org/10.5281/zenodo.17814769>
- 516 Rak, D. (2025). Southern Baltic Sea hydrographic CTD profiles along the Arkona–Bornholm–Ślupsk–Gdańsk  
517 transect (1997–2024). Geonetwork. <https://doi.org/10.48457/IOPAN.2025.531>
- 518 Rak, D., Przyborska, A., Bulczak, A. I., & Dzierzbicka-Głowacka, L. (2024). Energy fluxes and vertical heat  
519 transfer in the Southern Baltic Sea. *Frontiers in Marine Science*, 11, 1365759.  
520 <https://doi.org/10.3389/fmars.2024.1365759>

— sformatowano: Czcionka: (Domyślny) Arial

521 Rak, D., Walczowski, W., Dzierzbicka-Głowacka, L., & Shchuka, S. (2020). Dissolved oxygen variability in the  
522 southern Baltic Sea in 2013–2018. *Oceanologia*, 62(4, Part A), 525–537.  
523 <https://doi.org/10.1016/j.oceano.2020.08.005>

524 Rak, D., & Wieczorek, P. (2012). Variability of temperature and salinity over the last decade in selected regions  
525 of the southern Baltic Sea. *Oceanologia*, 54(3), 339–354. <https://doi.org/10.5697/oc.54-3.339>

526 Reissmann, J. H., Burchard, H., Feistel, R., Hagen, E., Lass, H. U., Mohrholz, V., Nausch, G., Umlauf, L., &  
527 Wieczorek, G. (2009). Vertical mixing in the Baltic Sea and consequences for eutrophication—A review.  
528 *Progress in Oceanography*, 82(1), 47–80. <https://doi.org/10.1016/j.pocean.2007.10.004>

529 Stigebrandt, A., & Gustafsson, B. (2003). The response of the Baltic Sea to climate change – Theory and  
530 observations. *Journal of Sea Research*, 49(4), 243–256. [https://doi.org/10.1016/S1385-1101\(03\)00021-2](https://doi.org/10.1016/S1385-1101(03)00021-2)

531 Walczowski, W., Merchel, M., Rak, D., Wieczorek, P., & Goszczko, I. (2020). Argo floats in the southern Baltic  
532 Sea. *Oceanologia*, 62(4, Part A), 478–488. <https://doi.org/10.1016/j.oceano.2020.07.001>